



Numerical study on the behavior and design of screw connected built-up CFS chord studs

Smail Kechidi¹, David C. Fratamico², José M. Castro³,
Nouredine Bourahla⁴, and Benjamin W. Schafer⁵

Abstract

This paper presents the development and validation of a finite element (FE) modeling protocol for screw connected, back-to-back built-up cold-formed steel (CFS) columns using results from experiments conducted at Johns Hopkins University. The shell finite element-based models have been constructed in the ABAQUS FE software and include non-linear geometric, material, and contact behavior. A unique feature of the model is the inclusion of a User Element subroutine (UEL) for the screw-fastener connections. This UEL can reproduce strength and stiffness deterioration under monotonic load as well as the pinching effect that occurs in the shear behavior of steel-to-steel and steel-to-wood connections when subjected to cyclic loading. Sixteen monotonic, concentric compression tests on two different built-up CFS cross-section sizes with varying fastener layouts and sheathing conditions were simulated. Good agreement is achieved between experimental and numerical results in terms of the prediction of strength and limit states. Based on a parametric study, the results indicate that under the tested end boundary conditions there is no significant boost in axial capacity with the addition of member end fastener groups at the top and bottom of the columns. Furthermore, the assessment of the loading demand on screw-fastened connections reveals the conservatism in built-up column fastener layout and design as required by AISI S100 (2016) section I1.2. The goal of this study is to examine the buckling, peak and post-peak behavior of built-up CFS columns, with both an experimental and a numerical approach to improve or augment existing design guidelines in which all relevant failure modes are considered in the design of built-up CFS columns. In addition, the characterization of monotonic and cyclic behavior is sought such that chord stud buckling limit states could be captured in seismic simulation of CFS-framed shear walls.

1. Introduction

Built-up cold-formed steel (CFS) members are often assembled and used in low to mid-rise CFS-framed buildings where higher axial capacity or greater local system rigidity is required. Typical

¹ Ph.D. Student, Dept. of Civil Engineering, University of Blida 1, <skechidi@yahoo.com>

² Ph.D. Student, Dept. of Civil Engineering, Johns Hopkins University, <fratamico@jhu.edu>

³ Professor, Dept. of Civil Engineering, University of Porto, <miguel.castro@fe.up.pt>

⁴ Professor, Dept. of Civil Engineering, University of Blida 1, <nbourahla@univ-blida.dz>

⁵ Professor, Dept. of Civil Engineering, Johns Hopkins University, <schafer@jhu.edu>

examples include chord studs in CFS-framed shear walls, truss members, and headers/jambes. Although built-up sections can be composed of many different cross-section types and in many different shapes, typical built-up sections include the back-to-back “I” and toe-to-toe “box” sections, which are doubly symmetric and are assembled using traditional CFS lipped channel sections. These built-up sections can offer an axial compression capacity of more than twice that of the individual members if composite action is developed via the stud interconnectors, which can be screws, bolts, welds, or battens. The numerical work presented in this paper is grounded in the tests of back-to-back built-up CFS columns conducted at Johns Hopkins University (Fratamico et al. 2016).

Although research on built-up CFS members has increased in the last decade, design rules for these types of members are still limited in current CFS specifications (eg. AISI S100). A limited series of column experiments with back-to-back CFS channel sections found that the AISI S100 modified slenderness ratio can be overly conservative and that end connections are critical for maintaining overall column strength (Stone and LaBoube 2005). Maia et al. (2016) studied partially composite CFS double angle sections experimentally and numerically, finding that batten interconnections significantly boost capacity in eccentrically loaded sections. Other experimental tests, conducted in parallel with numerical analysis at KU Leuven in a large research thrust, on various types of built-up CFS column cross-sections using Z-shaped studs have been completed (Georgieva et al. 2012). Axial capacities were compared with Direct Strength Method (DSM) based equations, calibrated to account for buckling interactions. Zhang (2014) completed similar testing of varying cross-sections; efficient attempts to model web interconnections were explored and new DSM equations were proposed. Craveiro et al. (2016) also completed tests and follow-up numerical models using back-to-back and closed section built-up CFS columns, and determined capacities at lower and upper bounds using pin and fixed ends, respectively. AISI and Eurocode predictions of strength were deemed conservative for fixed-ended columns, which is also seen in the column tests reported here. Sheathed built-up columns have not been studied in depth, but Vieira (2011) conducted work on the axial compressive capacity of sheathed single studs as part of a larger effort to study CFS walls sheathed with gypsum board and oriented strand board (OSB). Ye et al. (2016) conducted 16 full-scale column tests using single and back-to-back sections with OSB sheathing and observed local and flexural-torsional buckling deformation modes, which are not addressed in current design codes. These results are also confirmed by the experimental results reported herein. Berwick and Williamson (2014) used finite element models to study the blast resistant design of CFS wall systems. They used discrete beam elements to model all screw fasteners and found that the out-of-plane performance of CFS walls is highly dependent on the stud-to-track screw strength and failure mode; they were not able to use actual fastener stiffness and strength data from tests.

Discrete fastener models are useful in both CFS system and subsystem modeling, and real data on fastener performance and strength is desirable in finite element-based models. A first attempt to model discrete fasteners using elastic springs was done by Fratamico et al. (2015) to understand the effect of varying fastener spacing and stiffness on the composite action in built-up columns in an elastic flexural buckling study. Some work on the shear behavior of screw connections in CFS structures was performed by Ye et al. (2016) in which a parametric study on sheathing material and orientation, stud thickness, screw diameter, edge distance, and loading type revealed a panoply of deformation modes and cyclic behavior, and warranted further experimentation and numerical modeling. Significant strides were made by Moen et al. (2016) and Tao et al. (2016) on fastener

testing and modeling. A large parametric study on the monotonic and cyclic testing of screw connections for steel-steel, steel-OSB, and steel-gypsum board combinations was completed, with varying sizes of steel ply thickness and screw diameters. Test data for each combination was converted into a simple pinching model for use in numerical models. From the same research group, Ding (2015) created a unique user-defined element (UEL) for use in ABAQUS models as a subroutine, based on a Pinching4 framework (Lowes et al. 2003). This user-defined element was modified for the work presented herein. Similarly, Kechidi and Bourahla (2016) developed hysteresis models that were validated and implemented in OpenSees software for use in CFS shear wall simulations under monotonic and cyclic lateral loading; although the models prove useful, a caveat is that chord stud buckling cannot be included in the simulations.

The motivation for the experimental and numerical work presented in this paper is to study the composite action, prevailing buckling modes, post-peak behavior, and failure modes of a series of 16 built-up CFS columns. The goal is to specifically understand which components of a column, as constructed and installed in a traditional CFS structure, affect the composite action under concentrically applied compressive loads. Advanced shell finite element models, validated with test results, are completed in ABAQUS with nonlinear geometry, material, fastener, and contact behavior. These models can be used in successive studies and in lieu of further testing. Further, the characterization of monotonic and cyclic behavior is sought such that chord stud buckling limit states could be captured in CFS-framed walls.

2. Experimental Work on Built-Up Cold-Formed Steel Columns

2.1 Experimental Setup

Composite action was studied in previous experimental work by incrementally adding components to the test specimens: first a single stud with typical stud-to-track screw connection (the control case), then a built-up section without interconnections, then the addition of web screws with an even spacing calculated using section I1.2 of AISI S100 (2016), and then the addition of column end fastener groups (EFG) on the web and at the top and bottom ends and addition of sheathing on either flange of the built-up section (Fratamico et al. 2016). Figure 1 shows the back-to-back cross-section studied as well as the general layout of the EFG. The test series included monotonic, concentric compression loading using a 445 kN [100 kip] MTS universal testing rig, as shown in Figure 2. The column specimens were installed within tracks, which rested on fixed and parallel platen supports. Prevailing deformation modes and ultimate capacities for the 1.83 m [6 ft] long columns were observed for each specimen type.

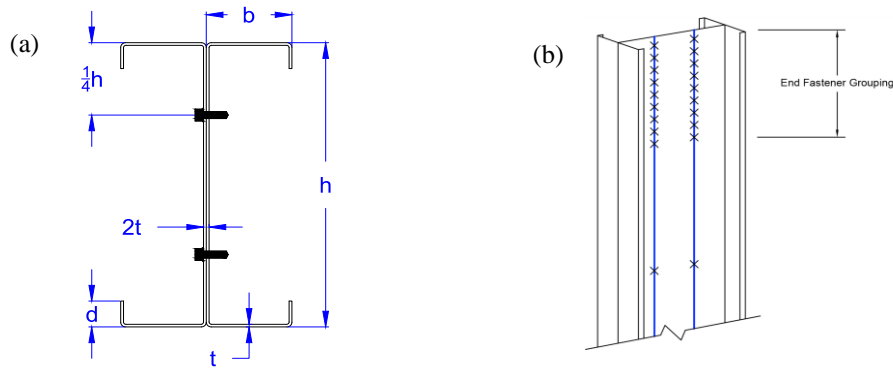


Figure 1. The nominal back-to-back cross-section studied with web screws shown (a) and end fastener groups (b)

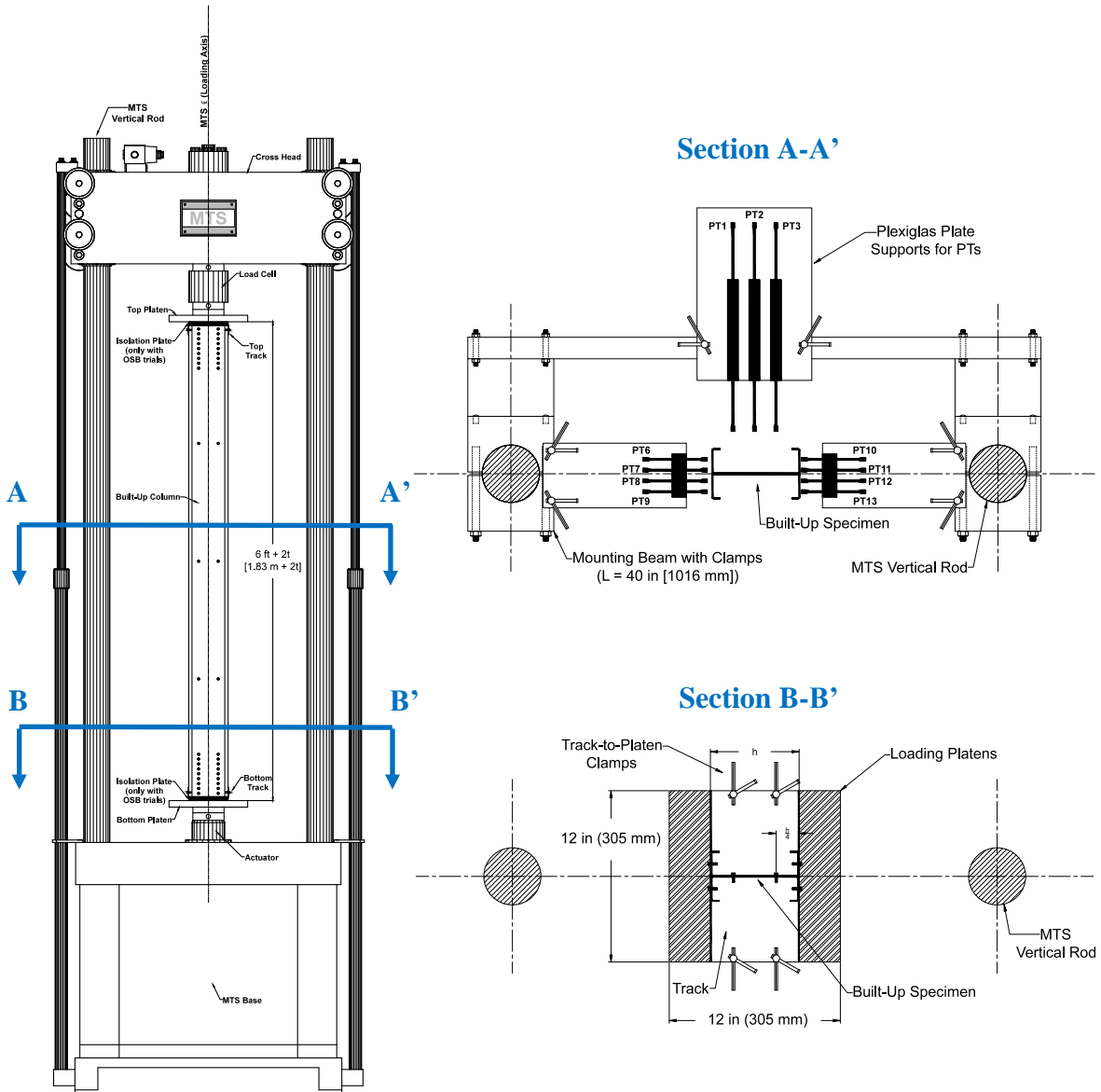


Figure 2. MTS testing rig (Fratamico et al. 2016) with specimen installed (left), position transducer arrangement at mid-height (Section A-A'), and specimen positioning on loading platens (Section B-B')

Two lipped channel sections are used in the test series: 362S162-68 and 600S137-54 (per AISI-S200-12 nomenclature). The 362S162-68 has a 3.625 in. [92.1 mm] deep web, 1.625 in. [41.3 mm] wide flange, and a nominal material thickness of 0.068 in. [1.73 mm]); the 600S137-54 section has a 6 in. [152.4 mm] deep web, 1.375 in. [34.9 mm] wide flange, and a nominal material thickness of 0.054 in. [1.37 mm]). Section types were selected based on local and distortional slenderness, yet they are all globally slender such that global buckling prevails at the tested length. Tests include single studs and doubled studs with varying web interconnection layouts (using #10 self-drilling screws), with all columns built with and without OSB sheathing. A full description and illustration of the test series are provided in Fratamico et al. (2016). Table 1 outlines the parametric study and specimen details are shown in Figure 3.

Table 1. Test matrix

Trial	Section Used		Sheathing	Single Stud	Built-Up Screw Layout		
	362S162-68	600S137-54			None	Even ^a	AISI ^b
A1	X			X			
A2	X				X		
A3	X					X	
A4	X						X
A5	X		X	X			
A6	X		X		X		
A7	X		X			X	
A8	X		X				X
B1		X		X			
B2		X			X		
B3		X				X	
B4		X					X
B5		X	X	X			
B5b ^c		X	X	X			
B6		X	X		X		
B7		X	X			X	
B8		X	X				X

^aEvenly-spaced screws along the length

^bPrescriptive AISI-based screw spacing

^cStaggered screw layout (illustrated in Figure 3c)

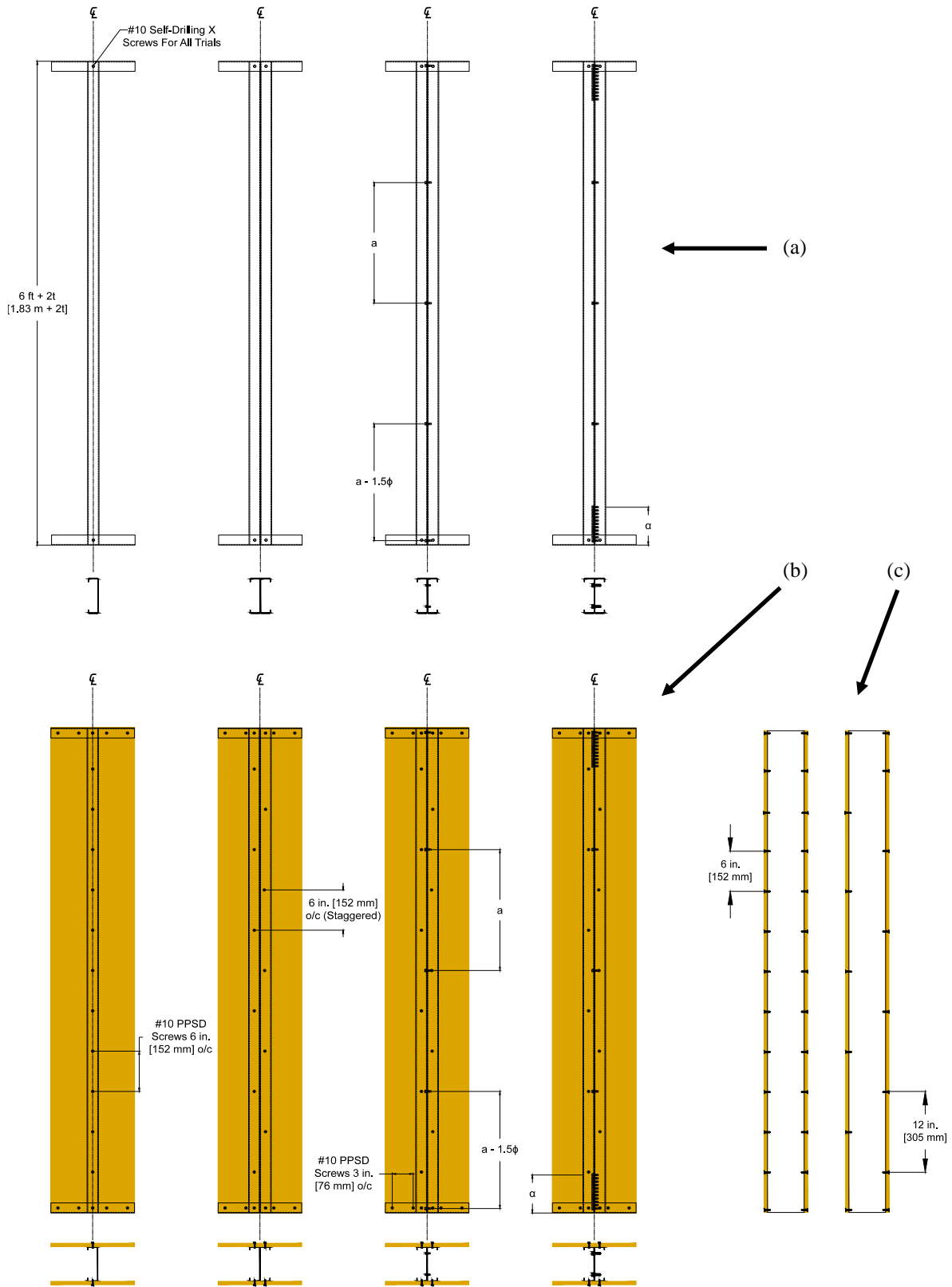


Figure 3. All 8 test specimens per section type: (a) unsheathed and (b) sheathed; (c) screw spacings for B5 and B5b

2.2 Summary of Test Results

Tested capacities and failure modes are shown in Table 2. Trials A1, A3, A4, and B1, as reported in Fratamico et al. (2016), have been updated with data from recent re-tests of the specimens. To view videos for all trials, visit <http://tinyurl.com/hhg3fn2>. Unsheathed specimens showed a wide range of buckling behavior: flexural minor axis, flexural-torsional, and distortional; while for the sheathed columns, local web buckling controlled since flanges were braced longitudinally with steel-OSB screws. The EFGs were shown to increase flexural buckling capacity in the unsheathed columns, but not in sheathed columns, as local failures dominated. See Fratamico et al. (2016) for further details.

Table 2. Summary of tested capacities

Trial	Specimen Type	Buckling Mode	P_u (kN) [kips]	Failure Mode
A1	Single 362S162-68	FT	91.93 [20.67]	FT
A2	Back-to-Back 362S162-68	FT ^a	194.3 [43.68]	FT ^a
A3	Back-to-Back 362S162-68	F ^b	187.4 [42.12]	L (web) ^a
A4	Back-to-Back 362S162-68	F ^b	219.8 [49.41]	L (web) ^a
A5	Single 362S162-68	L (web)	128.4 [28.87]	L (web)
A6	Back-to-Back 362S162-68	L (web) ^a	246.0 [55.31]	L (web) ^a
A7	Back-to-Back 362S162-68	L (web) ^a	236.9 [53.25]	L (web) ^a
A8	Back-to-Back 362S162-68	L (web) ^b	243.1 [54.66]	L (web) ^b
B1	Single 600S137-54	F	36.38 [8.179]	L (lips)
B2	Back-to-Back 600S137-54	F ^b	72.15 [16.22]	D/L ^a
B3	Back-to-Back 600S137-54	F ^b	75.98 [17.08]	D/L ^a
B4	Back-to-Back 600S137-54	L (web) ^b	87.63 [19.70]	D/L ^b
B5	Single 600S137-54 ^c	L (web) ^a	81.62 [18.35]	L (web)
B5b	Single 600S137-54 ^d	L (web) ^a	75.08 [16.88]	L (web)
B6	Back-to-Back 600S137-54	L (web) ^a	121.5 [27.31]	L (web) ^a
B7	Back-to-Back 600S137-54	L (web) ^a	134.6 [30.25]	L (web) ^a
B8	Back-to-Back 600S137-54	L (web) ^a	140.3 [31.53]	L (web) ^b

^aindependent buckling of the webs

^bcompatible buckling mode of the webs

^c6 in. even screw spacing connecting flanges and OSB board along the length

^d12 in. staggered screw spacing (from flange to flange) connecting flanges and OSB board, as required by AISI S100 (2016)

Note: *F* = minor axis flexural, *FT* = flexural-torsional, *L* = local, and *D* = distortional

3. Nonlinear Finite Element Modeling

The commercial finite element software ABAQUS 6.14-2 (Simulia 2014) was used to simulate the tested specimens and support conditions. The model and its parts are illustrated in Figure 4. The dimensions of the assembly are established per the previously described experimental setup. The following sections outline the modeling, including details on the material model, simulation of geometric imperfections, contact modeling, replication of end conditions from the test setup, and solution method.

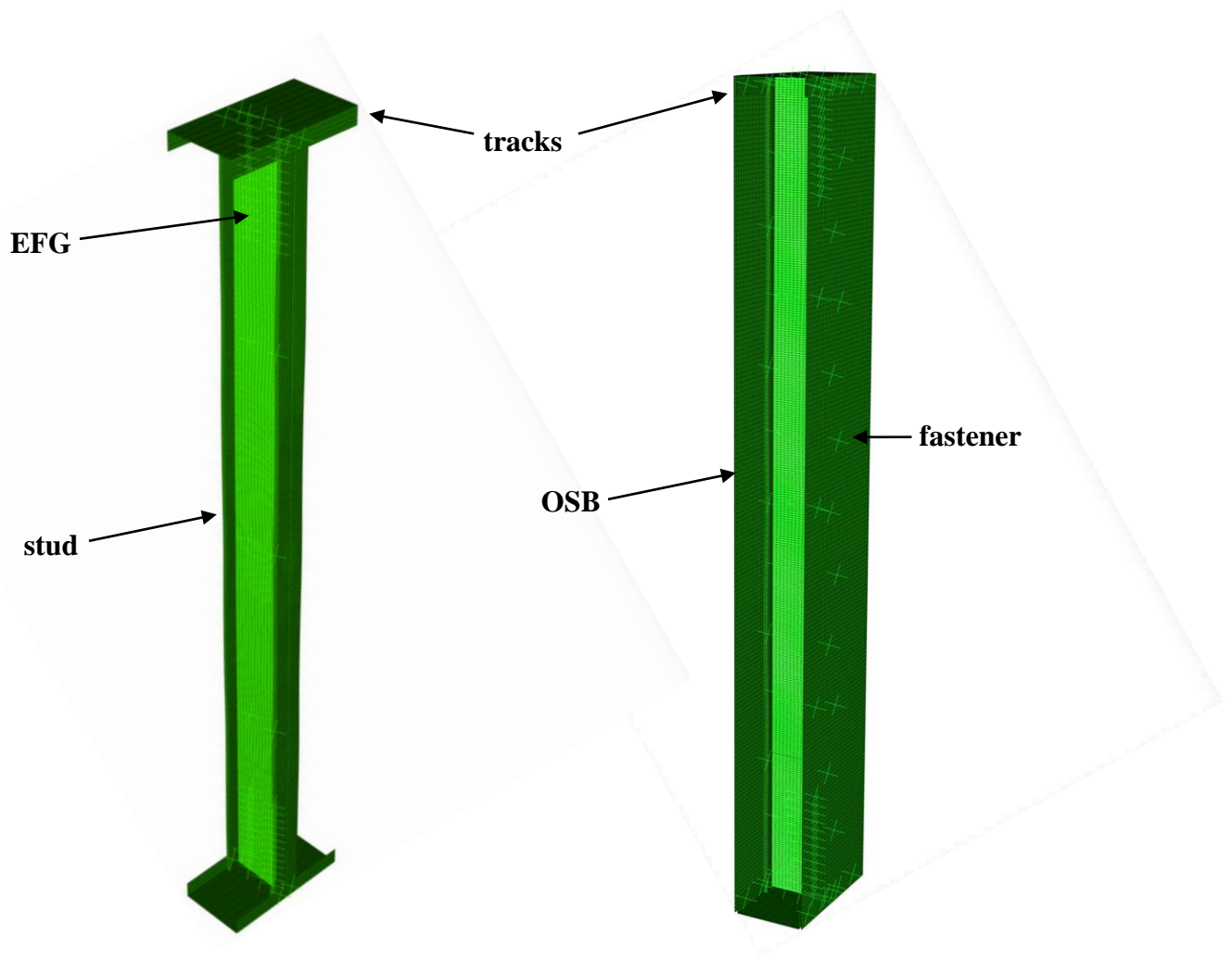


Figure 4. Undeformed ABAQUS models for specimens B4 (left) and B8 (right), showing the location of fasteners

3.1 Element Type and Mesh Generation

CFS studs and sheathing are modeled using nine-node quadratic, isoparametric shell finite elements known as S9R5 in ABAQUS. The element uses quadratic shape functions, employs a reduced integration scheme, and converges to Kirchhoff plate theory for thin plates. Five integration points are used through the thickness of the element, since no residual stresses are modeled in this work. Schafer et al. (2010) studied the sensitivity to element choice and mesh type in the computational modeling of CFS members and demonstrated that the mesh density has a great impact on the response of CFS members in finite element analyses. A coarse mesh can be adequate for capturing the distortional and global buckling modes, but typically cannot accurately reproduce local buckling modes. On the other hand, a medium or fine mesh can represent all buckling modes including local, distortional, and global with reasonable accuracy but at the expense of added computational time. Therefore, as depicted in Figure 4, a relatively fine mesh is used in this study. Signature curve analyses using a semi-analytical finite strip method-based elastic buckling software CUFSM (Schafer and Adány 2006) is used to generate the mesh for nominal geometries of each specimen and their corresponding local, distortional, and global buckling mode shapes for use in generating geometric imperfections (described in the following sections). Element are placed every 5 mm along the longitudinal axis of the built-up sections and

tracks, and 10 mm along the length for the OSB boards. This mesh discretization allows for four elements on the lip and flanges of the channel sections, and 8 and 16 elements on the web for the 362S162-68 and 600S137-54 sections, respectively. The aspect ratio of these elements is kept as close to 1:1 as practical and never exceeds 2:1. Corners are modeled with 4 elements.

3.2 Material Model

A series of tensile tests were completed to characterize basic material properties of the steel used in the two cross-section types of the test series. Testing was completed in accordance with ASTM A370-12a (2012), and results are shown in Table 3. Average yield stress (determined using the 0.2% offset method) for the 362S162-68 and 600S137-54 sections were recorded with a mean of 419.5 MPa [60.85 ksi] and 394.8 MPa [57.26 ksi], respectively, and were both larger than nominal 344.7 MPa [50 ksi]. Young’s modulus was not estimated from the test results and was assumed to be 29,500 ksi [203.4 GPa] as prescribed in AISI S100 (2016).

Table 3. Tensile test results

Specimen	Base Metal Thickness, t (mm) [in.]	Yield Stress, F _y (MPa) [ksi]	Tensile Strength, F _u (MPa) [ksi]
362S162-68-W1	1.82 [0.0717]	426.3 [61.83]	550.9 [79.90]
362S162-68-W2	1.83 [0.0719]	420.7 [61.02]	540.1 [78.34]
362S162-68-F1	1.85 [0.0727]	428.6 [62.17]	546.7 [79.29]
362S162-68-F2	1.81 [0.0713]	402.4 [58.37]	535.9 [77.73]
Mean	1.83 [0.0719]	419.5 [60.85]	543.4 [78.81]
C.o.V.	0.008	0.028	0.012
600S137-54-W1	1.40 [0.0551]	402.3 [58.35]	484.5 [70.27]
600S137-54-W2	1.40 [0.0551]	398.1 [57.74]	481.0 [69.77]
600S137-54-F1	1.39 [0.0546]	389.4 [56.48]	481.8 [69.87]
600S137-54-F2	1.38 [0.0544]	389.4 [56.48]	480.7 [69.72]
Mean	1.39 [0.0548]	394.8 [57.26]	482.0 [69.91]
C.o.V.	0.006	0.016	0.004

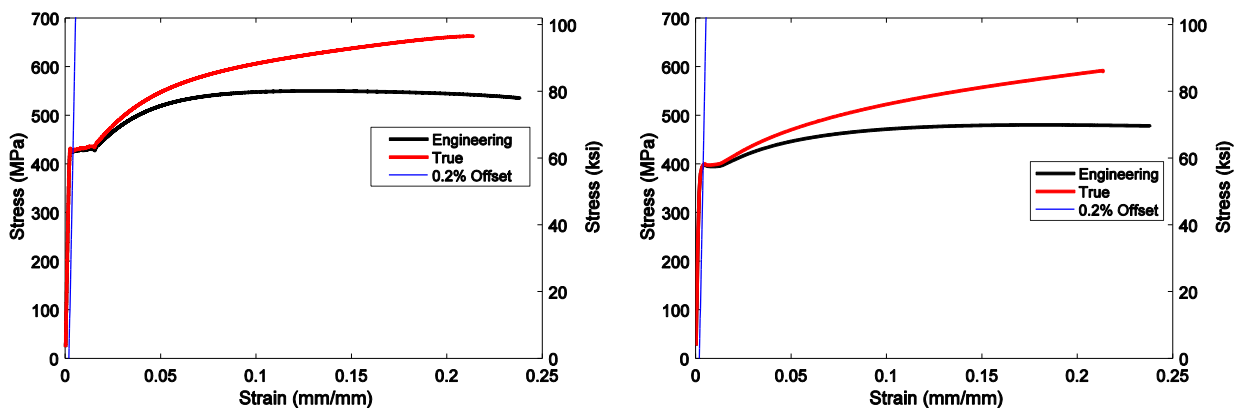


Figure 5. Stress vs. strain for coupons cut from the webs of the 362S162-68 (left) and 600S137-54 section (right)

Selecting data from tests in which web-cut coupons were used and the average yield stress was attained as shown in Figure 5. A material model using classical von Mises plasticity with isotropic hardening was selected. Raw data was recorded as engineering stress and engineering strain, and

therefore conversions to true stress and true, plastic strain at 20 discrete points from the plotted curves were determined using Equations 1 and 2:

$$\sigma = s(1 + e) \quad (1)$$

$$\varepsilon_{plastic} = \ln(1 + e) - \frac{\sigma}{E} \quad (2)$$

where engineering stress and engineering strain are denoted as s and e , respectively. Young's modulus is E , and true stress and true strain are σ and ε , respectively. $\varepsilon_{plastic}$ is the true, plastic strain (without the elastic strain component, which was subtracted at each point). Table 4 shows the set of 20 data points used in the ABAQUS analyses.

Table 4. Plastic material parameters used in ABAQUS for both cross-section types

362S162-68 Section		600S137-54 Section	
Stress (MPa) [ksi]	Strain (mm/mm)	Stress (MPa) [ksi]	Strain (mm/mm)
420.9 [61.04]	0.0000	390.0 [56.57]	0.0000
421.1 [61.08]	0.0005	392.2 [56.88]	0.0009
421.7 [61.16]	0.0006	400.6 [58.10]	0.0024
422.4 [61.27]	0.0011	400.7 [58.11]	0.0025
423.1 [61.37]	0.0033	399.8 [57.99]	0.0031
425.0 [61.63]	0.0067	399.6 [57.95]	0.0032
425.4 [61.69]	0.0095	398.4 [57.78]	0.0044
425.0 [61.63]	0.0109	399.4 [57.93]	0.0077
437.8 [63.49]	0.0140	400.5 [58.09]	0.0095
490.7 [71.17]	0.0275	415.2 [60.22]	0.0168
532.6 [77.24]	0.0441	451.7 [65.51]	0.0348
545.0 [79.04]	0.0510	460.5 [66.78]	0.0402
560.1 [81.24]	0.0613	488.2 [70.80]	0.0610
576.0 [83.55]	0.0751	514.7 [74.65]	0.0872
591.4 [85.78]	0.0924	519.7 [75.37]	0.0928
602.7 [87.42]	0.1077	531.2 [77.04]	0.1071
613.0 [88.90]	0.1236	552.6 [80.15]	0.1379
627.8 [91.06]	0.1513	567.6 [82.32]	0.1627
629.6 [91.31]	0.1556	580.8 [84.23]	0.1869
620.8 [90.04]	0.1616	591.8 [85.83]	0.2082

3.3 Consideration of Geometric Imperfections

Geometric imperfections were incorporated into the finite-element models using the buckled shapes of single and back-to-back sections analyzed in CUFSM with a signature curve analysis (Schafer and Ádány 2006). Nominal section sizes were used, but measured values were used for the thickness. For efficiency in modeling the back-to-back sections, webs were constrained to move in a compatible mode in all buckled shapes; where the two fasteners were located on the web, a master-slave type constraint was used to tie the webs together. Both shapes and wavelengths were preserved from CUFSM for the imperfection fields for the local and distortional modes for all section types considered, and one half sine wave (mode 1) was used for the minor-axis global mode (G1) for the single and built-up 600S137-54 section. For the flexural-torsional imperfection required for the 362S162-68 single and built-up sections, the superposition of a half sine wave of

major-axis/camber (G2) with a full cosine wave of pure torsional (G3) mode was used, as recommended by Zhao (2016). An in-house MATLAB code was used to transcribe buckled shape information into shell finite element meshes using the corresponding imperfection mode shapes for each specimen, with all four shapes shown in Figure 6.

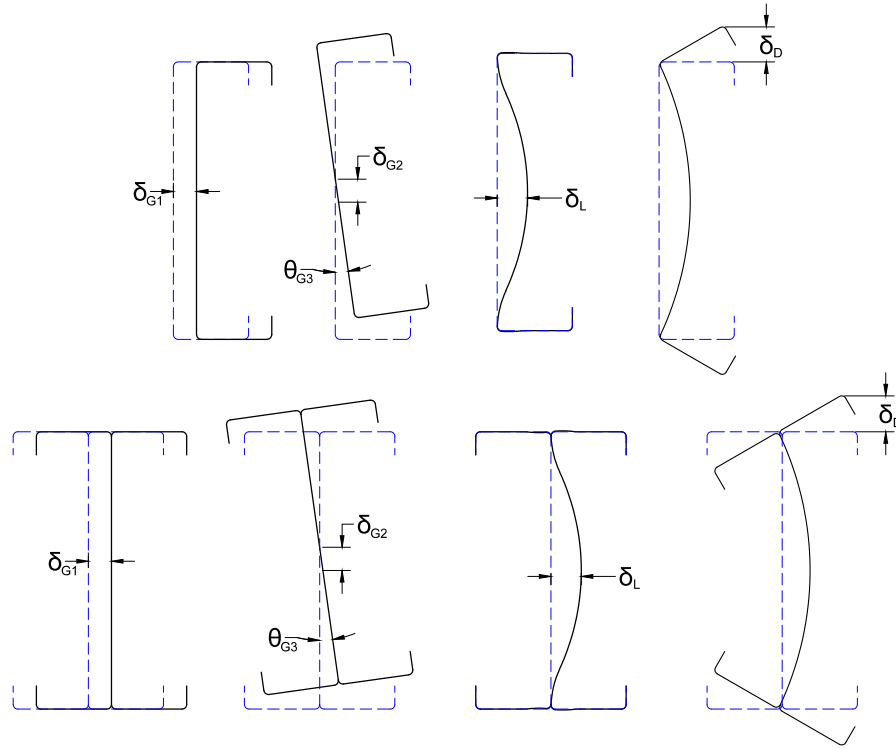


Figure 6. Mode shapes for single sections (top row) and built-up sections (bottom row) used in creating modal imperfections in ABAQUS models; the positive orientation of each shape is shown from left to right: single global minor axis (G1), flexural-torsional (G2+G3), local (L), and distortional (D).

The amplitudes δ_{G1} , δ_{G2} , θ_{G3} , δ_L , and δ_D are taken from databases developed using imperfection data for single sections specifically used in this study. A novel, in-house laser scanning rig at Johns Hopkins University was used to scan a sizeable number of the same single sections used in the study presented herein; full-field 3D geometric information was acquired and post-processed to assemble a statistical database of modal shape amplitudes based on a decomposition of the true, 3D geometries into the five buckling mode shapes: global (G1, G2, and G3), local, and distortional (Zhao 2016). This approach is known as the Modal Imperfection Decomposition (MID) method, and it is particularly useful since imperfections patterns are frequently affine to these five buckling mode shapes (Zeinoddini and Schafer 2012). Another statistical database of amplitudes was also used, which contains imperfection data from a “conventional” hand-measurement approach (Zhao 2016). In the conventional approach, the largest values of amplitude, obtained from measurements of the five imperfection modes along the length of a large sample of the 362S162-68 and 600S137-54 sections, are used. This method provides more conservative estimates of imperfection amplitudes.

Median buckling mode amplitudes are used from both the MID and conventional databases in this work, and the values are shown in Table 5. A total of eight possible combinations of both positive and negative global, local, and distortional modes are modeled using both MID and conventional amplitudes to find the specific combination which delivered model deformations and capacities most compatible with those observed in the tests. Using a small parametric study, deformation patterns that best matched tested behavior were obtained using specific combinations of imperfection modes for each specimen, as provided in Table 6.

Table 5. Median buckling mode amplitudes used

Cross Section	Imperfection Database	Local (Type 1)	Distortional (Type 2)	G1	G2	G3 ¹
362S162-68	Conventional	1.06t	0.93t	L/2271	L/2497	0.31L ²
	MID	0.58t	0.43t	L/2271	L/2497	0.31L
600S162-54	Conventional	0.97t	1.88t	L/863	L/2239	0.09L
	MID	0.95t	1.45t	L/863	L/2239	0.09L

¹G3 (torsional) imperfection amplitude is calculated in degrees

²member full length in feet

Table 6. Combination of imperfection orientations used for each simulated test specimen

Trial	G1	G2	G3	L	D	Trial	G1	G2	G3	L	D
A1*		+	+	-	-	B1	-			-	-
A2	+			+	+	B2	+			+	+
A3	+			+	+	B3	+			+	+
A4	+			+	+	B4	+			+	+
A5*		+	+	-	-	B5/B5b	-			-	-
A6	+			+	+	B6	+			+	+
A7	+			+	+	B7	+			+	+
A8	+			+	+	B8	+			+	+

*Flexural-torsional imperfection was modeled as a superposition of major-axis flexural and torsional modes

Furthermore, some important assumptions and simplifications of the imperfection modeling for back-to-back sections were made. As indicated earlier, the databases are developed from single section scan data. The assumption has two parts: (1) when single sections are combined to form a back-to-back section, the individual sections do not significantly change their shape as the webs are screw fastened together, and (2) as not enough built-up sections were scanned to create a separate database, imperfection amplitudes obtained from single stud scans are still meaningful and useable for the first mode buckled shapes of the built-up columns.

3.4 Implementation of User-Defined Elements as Screw Fasteners

ABAQUS has a comprehensive set of elements, nevertheless, there are still some types of elements not available in its element library for properly modeling fastener behavior, including loading and unloading paths. To overcome this limitation and achieve high-fidelity modeling applicable to both monotonic and cyclic analyses requires an extension to ABAQUS that incorporates empirical screw-fastened connection hysteretic loops and an algorithm resolving the bidirectional trajectory issue. Recent research carried out by Ding et al. (2015) resulted in an ABAQUS user-defined element (UEL) which incorporates the Pinching4 model (Lowe et al. 2003) which is capable of simulating strength and stiffness deterioration as well as the pinching effect observed in the response of screw-fastened connections. In this study, determination of the Pinching4 parameters

and implementation of the UELs are performed as follows. First, strength and stiffness backbones determined by Moen et al. (2016) and Tao et al. (2016) from the experimental results of steel-to-steel and steel-to-OSB screw fasteners tested in shear have been converted to Pinching4 parameters. Second, the loading and unloading parameters of the Pinching4 model are then fit such that the sum squared error in the energy for each loop is minimized. MATLAB was employed for minimizing the error, in conjunction with the simplex method employed in the *fminsearch* routine. This method ensures that strength and hysteretic energy are accurately captured.

The UEL has been verified at the connection level, including complex cyclic deformation paths (following the CUREE loading protocol) using a comparison with experimental test results. Figure 7 shows a sample of shear strength vs. lateral displacement hysteresis loops of a sample 33 mils [0.84 mm] steel-to-OSB screw fastener response from tests plotted with ABAQUS results. In general, acceptable correlation is observed in terms of strength (in-cycle) and stiffness deterioration, and the pinching effect is also recreated adequately. Calibrated Pinching4 parameters (shown in Table 7) are then directly input into the FORTAN subroutine which forms the basis of the UEL.

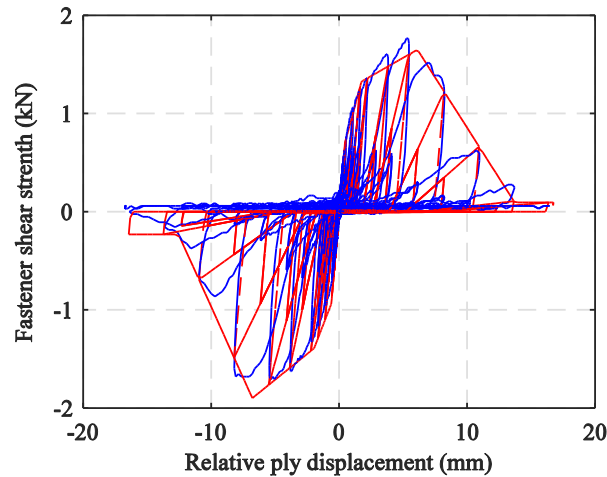


Figure 7. Comparison of tested shear force–deformation response (blue) with ABAQUS fitted Pinching4 model (red) for a 33 mils steel-to-OSB screw connection

In the models presented herein, the configuration of steel-to-OSB screw-fastened connections is either 54 or 68 mils [1.37 or 1.73 mm, respectively] to 7/16 in. [11 mm] OSB, and steel-to-steel screw-fastened connections for 54-to-54 mils [1.37 mm to 1.37 mm] and 68-to-68 mils [1.73 mm to 1.73 mm] combinations (Moen et al. 2016). To consider changes in displacement trajectory, a radial spring model is used for the UEL.

Table 7. Pinching4 characterization of fasteners

(a) Backbone Points*									
Steel Thickness (mm)	Connection	ePd ₁ (mm)	ePd ₂ (mm)	ePd ₃ (mm)	ePd ₄ (mm)	ePf ₁ (kN)	ePf ₂ (kN)	ePf ₃ (kN)	ePf ₄ (kN)
1.37	steel-steel	0.41	3.97	5.95	7.53	4.28	6.14	4.17	0.0001
1.37	steel-OSB	1.04	11.47	21.70	28.85	1.70	2.83	1.43	0.0001
1.73	steel-steel	0.25	1.73	2.33	2.80	6.43	8.16	6.62	0.0001
1.73	steel-OSB	1.00	12.37	23.07	29.05	2.00	3.40	1.75	0.0001

(b) Unloading and Reloading Parameters							
Steel Thickness	Connection	rDispP	rForceP	uForceP	rDispN	rForceN	uForceN
all	all	0.42	0.01	0.001	0.42	0.01	0.001

*Positive and negative directions are taken as numerically equivalent but opposite in sign

3.5 Interactions and Constraints

Surface-to-surface contact using the finite-sliding tracking method was used to define the interaction relationship between the webs of the channel sections and between the channel section flanges and the OSB when present. Interpenetration of these shell elements was prevented. The general contact algorithm uses a “hard contact” formulation and the penalty method is used to approximate the hard pressure-overclosure behavior. Friction was also modeled, and the friction coefficient is taken as 0.19 (for steel-steel and steel-OSB) per tests conducted by Ye et al. (2016).

3.6 Boundary Conditions, Loading Method, and Solution Scheme

The specimens were tested between fixed platens. Therefore, all degrees of freedom (DOF) of both top and bottom track webs of the specimen have been restrained using rigid body tie constraints to two reference points that coincide with top and bottom cross-section centroids of the column. All DOF of the two reference points have been restrained except for the translational DOF in the axial direction of the top end (to which the displacement loading is applied) to simulate a globally fixed, warping free boundary condition. The displacement boundary condition is applied downward at the top reference point. The column cross-section nodes, at both ends, are constrained to reference points using linear multi-point constraints.

Although the commonly used Static-Riks solver is typically preferred for static, monotonic loads applied to models with thin shell elements, convergence was difficult to achieve in most of the models. Therefore, the Dynamic-Implicit solver was adopted for this study. This solution technique is robust and can be used for problems involving large nonlinearities (material or geometric), contact modeling, and moderate energy dissipation. Results of peak capacity as well as load vs. axial deformation response using the Dynamic-Implicit solver compare well with corresponding results obtained using Static-Riks for models in which the latter method functioned without convergence issues. Specifically, for specimen A4, a 3% reduction in peak capacity is observed when using Static-Riks when compared to the peak load from a Dynamic-Implicit analysis; however, the Static-Riks based response curve did not proceed more than two increments beyond the peak load for lack of convergence and analysis termination.

4. Comparison of Modeling Results with Experimental Data

The proposed modeling protocol for the built-up CFS chord studs is validated using test data. Figure 8 shows comparisons between the measured monotonic response and that predicted by the FE simulation in terms of axial strength versus axial shortening curves for fully built-up columns A4 and A8 (unsheathed and sheathed back-to-back 362S162-68 sections, respectively), and B4 and B8 (unsheathed and sheathed back-to-back 600S137-54 sections, respectively).

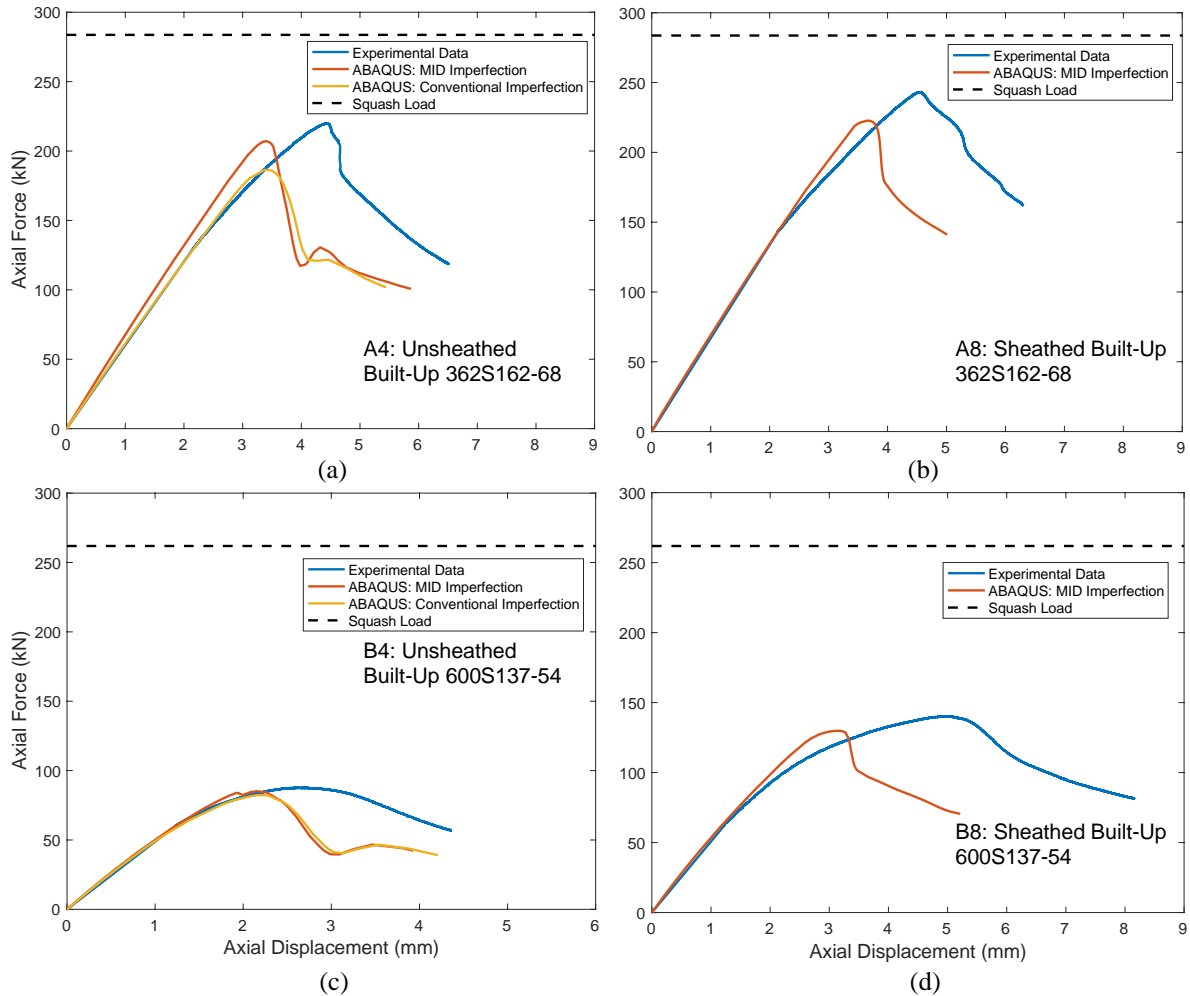


Figure 8. Plots of measured axial force vs. LVDT displacement for specimens A4 (a), A8 (b), B4 (c), and B8 (d)

From Figure 8, the FE predicted responses (using both conventional and MID type imperfection magnitudes) compare reasonably well with the measured ones. Some differences in displacement at peak loads are visible, particularly for the sheathed specimens A8 and B8 in Figure 8b and 8d. As the following ABAQUS output and test pictures for these specimens show, collapse modes as observed in the test were difficult to accurately model in ABAQUS. Nevertheless, using the MID type geometric imperfection characterization, a close agreement with ultimate strength was achieved. The plots also confirm that the FE modeling protocol is reliable for simulating monotonic behavior of back-to-back chord studs regardless of the chord stud's cross-section, geometry, fastener layout and the presence of sheathing.

The ultimate axial strength and the failure modes predicted by FEA are compared with the experimental results in Table 8. Generally, the ultimate axial strengths of the simulated specimens that were modeled having conventional type geometric imperfection amplitudes are more conservative, as expected, than in the cases in which MID amplitudes are modeled. Since MID results tend to be more accurate (with test to predicted ratios closer to 1.0) and for computational efficiency, only MID type imperfections were modeled for all sheathed specimens. Hereafter, only the numerical results using the MID approach are discussed.

Table 8. Comparison of test results with ABAQUS strength predictions

Trial	OSB ¹	Buckling Mode ²	Experiment P _{test} (kN) [kips]	ABAQUS P _u (kN) [kips]		P _{test} /P _u	
				Conventional	MID	Conventional	MID
A1	-	FT	91.93 [20.67]	87.73 [19.72]	97.07 [21.82]	1.05	0.95
A2	-	FT	194.3 [43.68]	185.4 [41.69]	204.9 [46.05]	1.05	0.95
A3	-	L-G	187.4 [42.12]	184.2 [41.42]	203.6 [45.78]	1.02	0.92
A4	-	L-G	219.8 [49.41]	186.5 [41.92]	207.2 [46.57]	1.18	1.06
Mean						1.07	0.97
C.o.V.						0.07	0.06
A5	yes	L	128.4 [28.87]	-	111.9 [25.15]	-	1.15
A6	yes	L	246.0 [55.30]	-	225.0 [50.58]	-	1.09
A7	yes	L	236.9 [53.26]	-	222.7 [50.06]	-	1.06
A8	yes	L	243.1 [54.66]	-	222.6 [50.05]	-	1.09
Mean						1.00	1.10
C.o.V.						0.08	0.03
B1	-	L-G	36.38 [8.179]	37.25 [8.374]	37.25 [8.374]	0.98	0.98
B2	-	L-D	72.15 [16.22]	67.04 [15.07]	67.11 [15.09]	1.08	1.08
B3	-	L-D	75.98 [17.08]	84.80 [19.06]	81.75 [18.38]	0.90	0.93
B4	-	L-D	87.63 [19.70]	82.33 [18.51]	85.13 [19.14]	1.06	1.03
Mean						1.00	1.00
C.o.V.						0.08	0.06
B5	yes	L	81.62 [18.35]	-	70.54 [15.86]	-	1.16
B5b	yes	L	75.08 [16.88]	-	67.76 [15.23]	-	1.11
B6	yes	L	121.5 [27.31]	-	129.5 [29.11]	-	0.94
B7	yes	L	134.6 [30.26]	-	129.5 [29.12]	-	1.04
B8	yes	L	140.3 [31.54]	-	129.9 [29.19]	-	1.08
Mean						1.00	1.06
C.o.V.						0.08	0.08

¹Sheathed with oriented strand board (OSB)

²FT=flexural-torsional, L-G=local-global interactive, L=local, and L-D=local-distortional interactive buckling

Observed failure modes at peak load from the test and FE specimens are listed in Tables 6. The unsheathed specimens (A1-A4 and B1-B4) failed by flexural torsional buckling (FT), flexural buckling (F), or local-distortional buckling (L-D) modes. Web local buckling (L) was the dominant failure mode for all sheathed specimens (A5-A8 and B5-B8). Generally, a good agreement was achieved between the test results and FE results in the post-buckling regime. Figures 9-12 show the failure modes at ultimate loads observed in the tests and predicted by the FE simulation for specimens A4, A8, B4, and B8. The ABAQUS outputs show von Mises stress contours on the shell element surfaces, with the grey regions indicating the yielded areas.

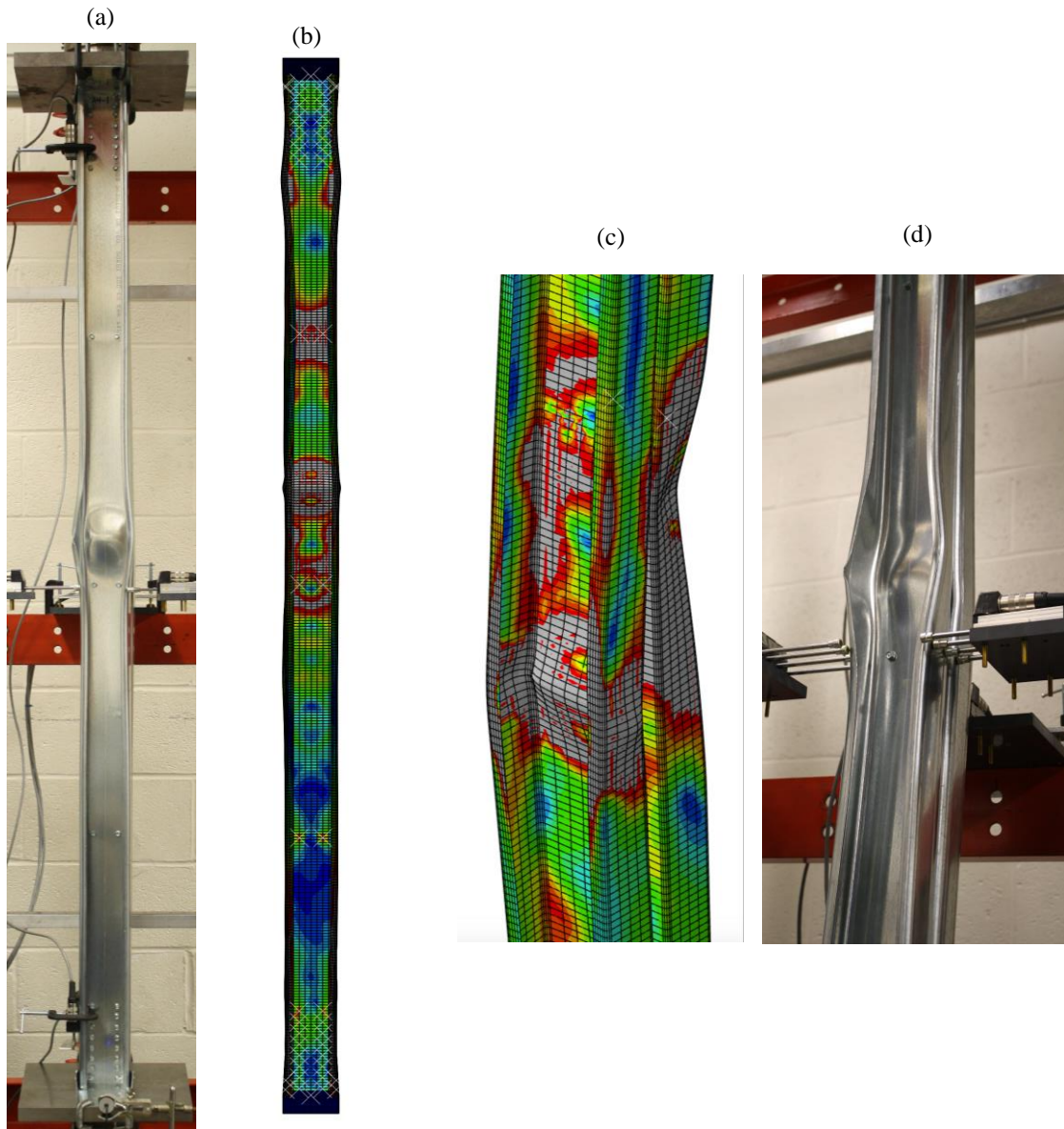


Figure 9. Tested (a) and numerical model (b) deformations at peak load for trial A4 showing global-local interaction, and a detailed view of plastic hinge formation in the numerical model (c) and in the tested specimen (d)

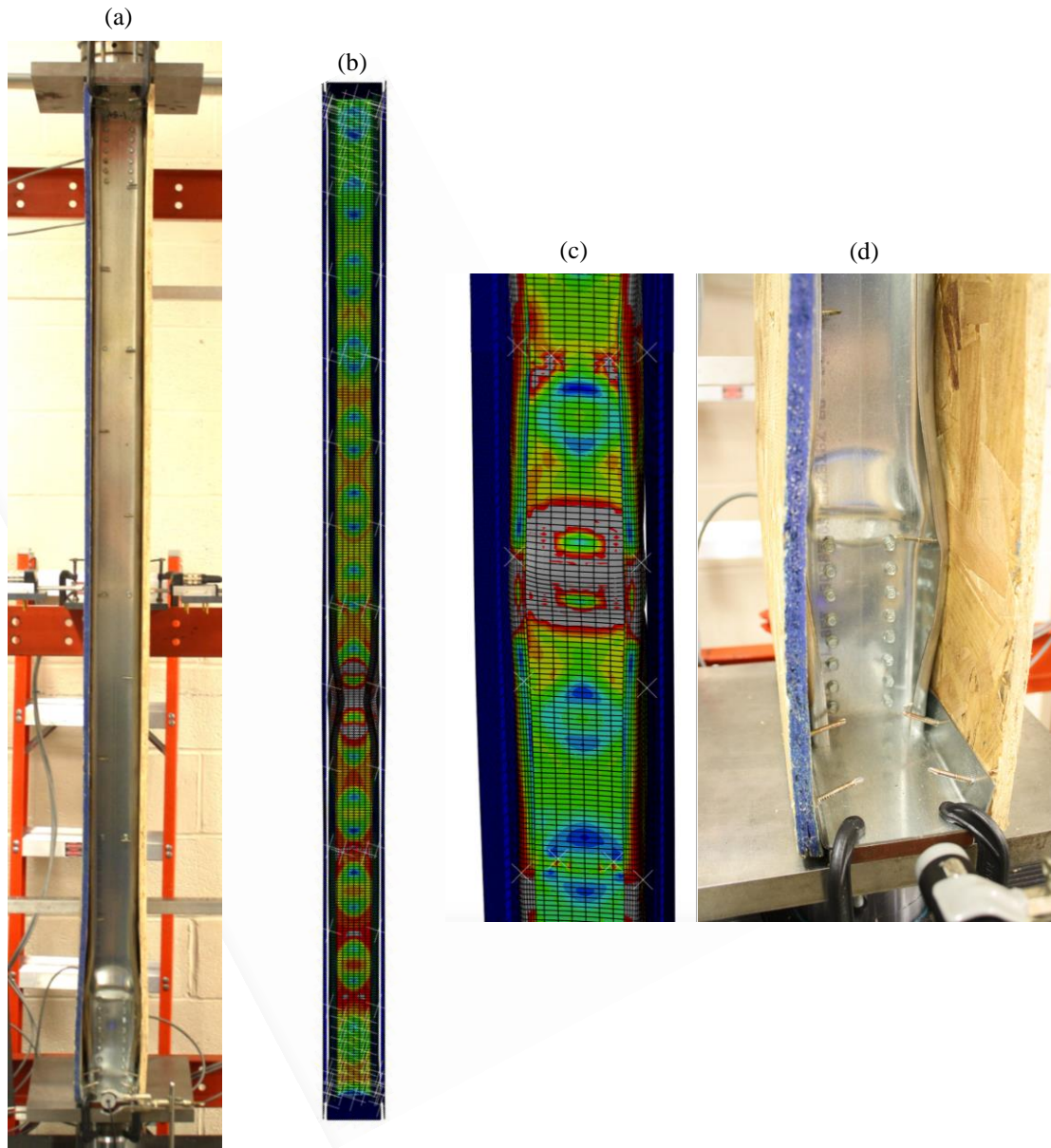


Figure 10. Tested (a) and numerical model (b) deformations at peak load for trial A8 showing a localized failure in the web, and a detailed view of plastic hinge formation in the numerical model (c) and in the tested specimen (d)

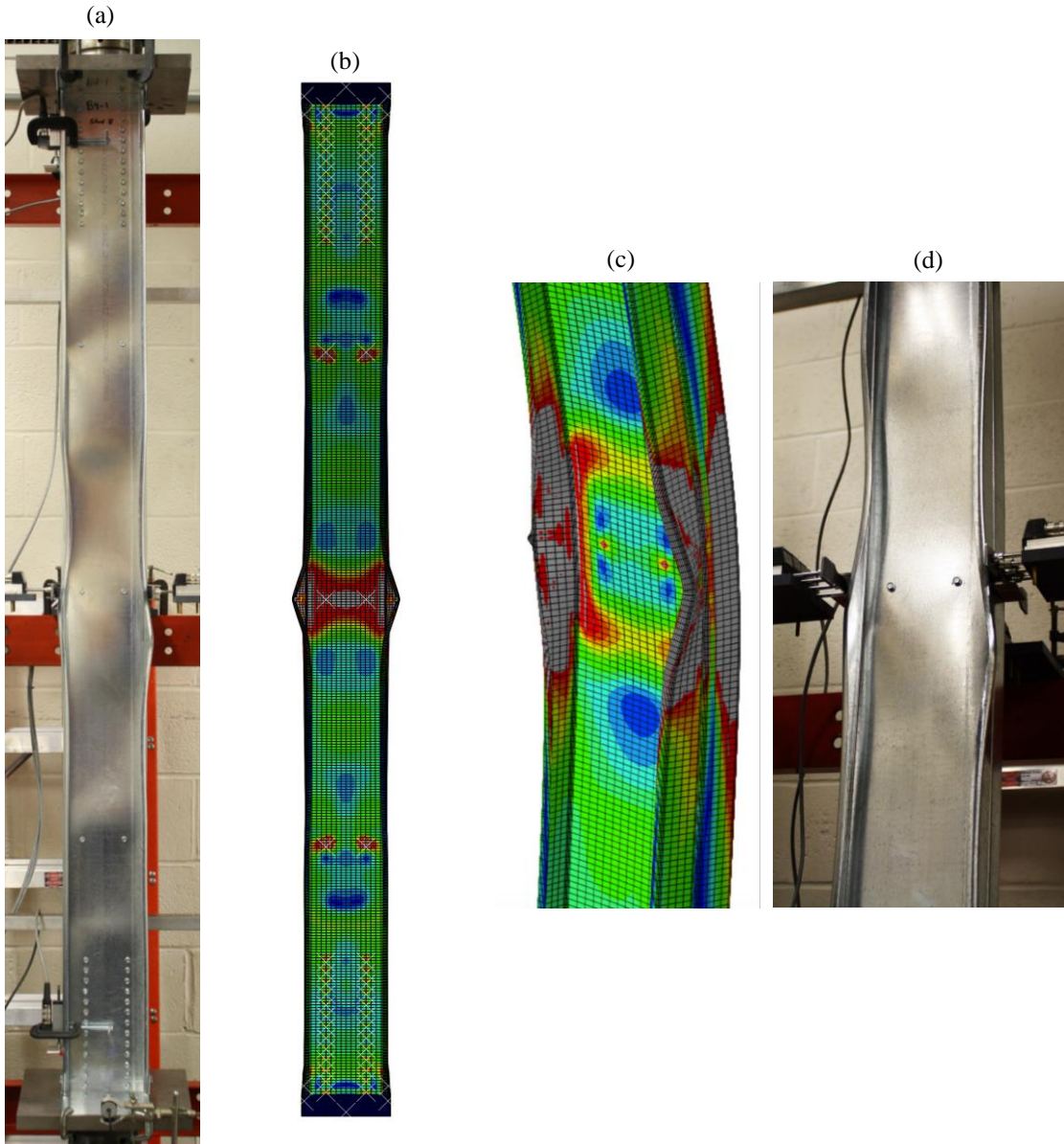


Figure 11. Tested (a) and numerical model (b) deformations at peak load for trial B4 showing global-local-distortional interaction, and plastic hinge formation in the numerical model (c) and in the tested specimen (d)

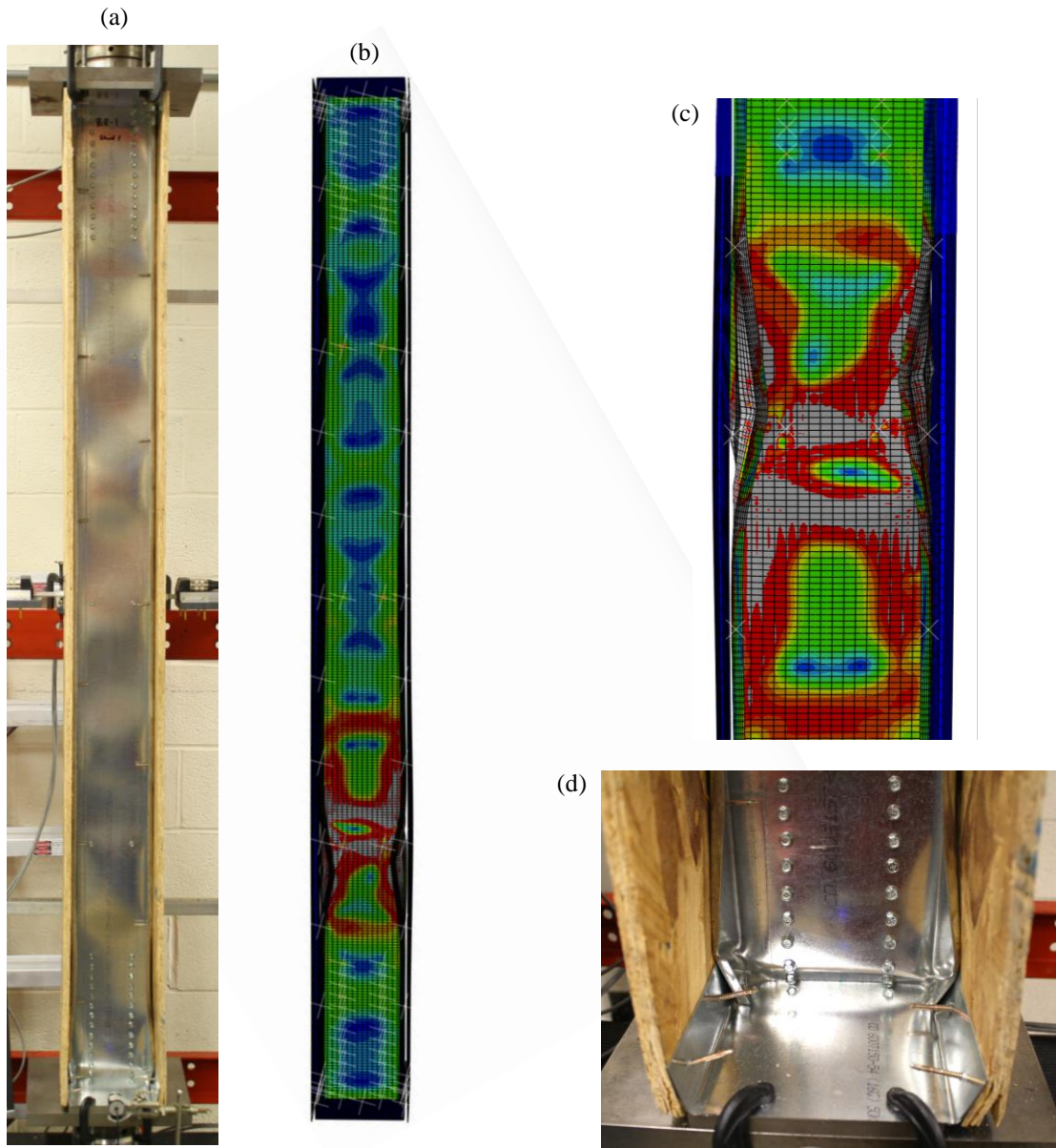


Figure 12. Tested (a) and numerical model (b) deformations at peak load for trial B8 showing localized web failure, and plastic hinge formation in the numerical model (c) and the tested specimen (d), although the location is different

5. Shear Demand on Screw Fasteners

In this study, no significant boost in axial capacity has been observed with the addition of EFGs at the top and bottom of the studied columns, particularly the sheathed ones (see Table 8). Additionally, the commentary of AISI S211-07 (2012) states that a fastener-sheathing assembly should be designed for a load equal to 2% of the axial load, also known as the “2% rule.” To assess such a statement as well as the validity of the fastener layout and design required by AISI S100 (2016) section II.2, the shear demand on screw fasteners at the peak axial capacity of the column is quantified in this section.

Figure 13 shows that the highest demand in the screw-fastened connections recorded at peak load in specimen B4 is very small compared to its capacity. The maximum shear strength of a screw connection for steel-to-steel is 6.14 kN [1.38 kips] and 8.16 kN [1.83 kips] for 54 mils (1.37 mm) and 68 mils (1.73 mm) plates, respectively. In the model, the maximum shear demand at the UEL with maximum force at peak load is recorded to be 0.14 kN [31.5 lbf] for unsheathed column and of 0.45 kN [0.10 kips] for sheathed column. These results shed light on the conservatism in built-up column fastener layout and design required by AISI S100 (2016) section II.2. As for OSB-to-steel connections, the maximum shear strength of the spring is 2.83 kN [0.64 kips] and 3.40 kN [0.76 kips] for 54 mils (1.37 mm) and 68 mils (1.73 mm) plates, respectively, while in the specimen B8 model, a typical shear demand at the spring is 39.8×10^{-6} kN [0.01 lbf], which is very small when compared to the 129.9 kN (29.2 kips) peak load of B8 with the MID-based imperfection.

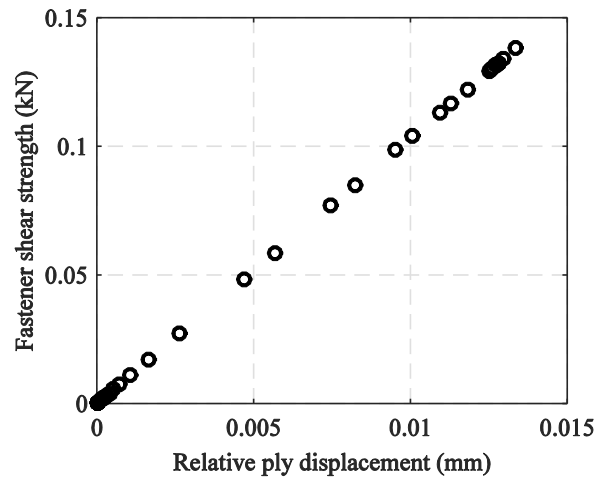


Figure 13. Linear shear response of screw fastener with highest force recorded at peak load in specimen B4

Figure 14 shows a distribution of shear forces from all web screws in specimen B4 at peak load. Specifically, the fastener forces are plotted on the ordinate as a percent of the peak load of specimen B4 from ABAQUS using the MID-type imperfection: 85.13 kN [19.14 kips]. Note that the screws in the EFG are collectively carrying most of the shear forces in the column in flexural buckling, but those screws each have small shear forces relative to their shear strength.

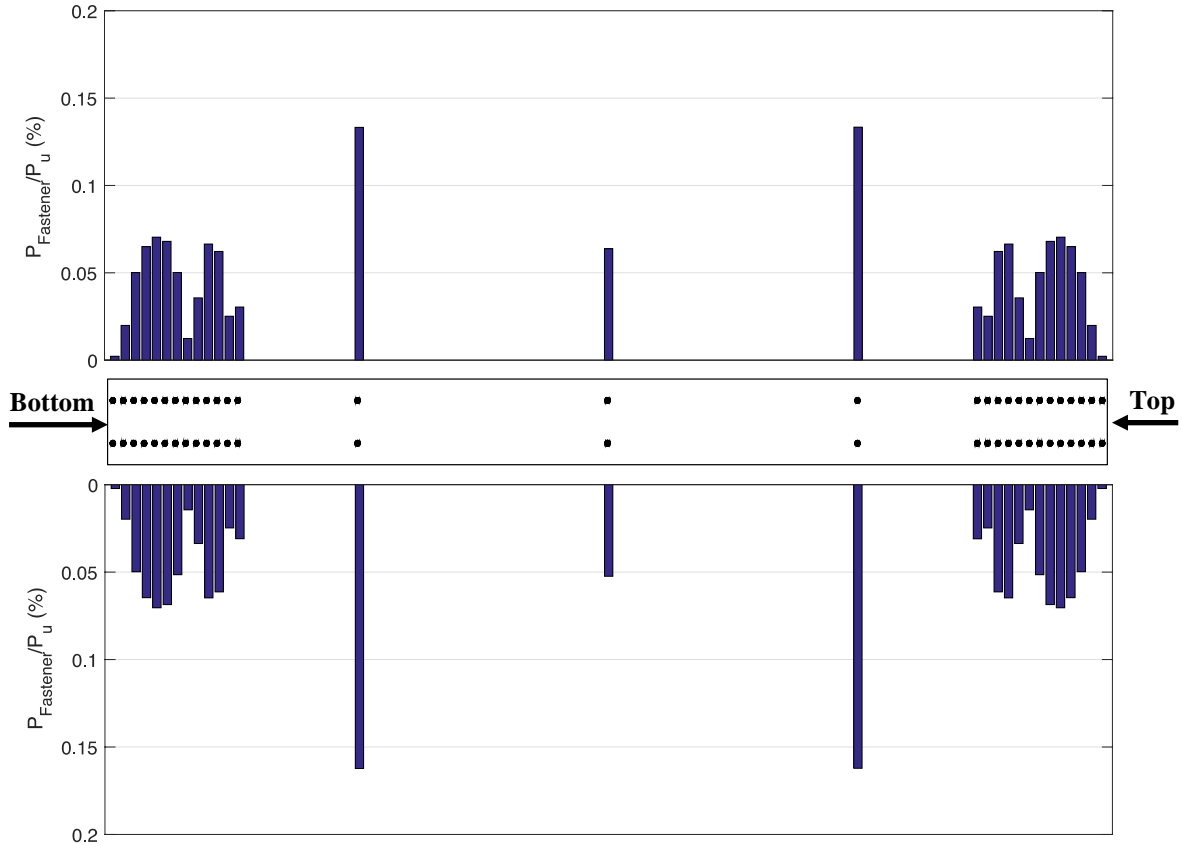


Figure 14. Peak shear demand on individual web screws in specimen B4

Screw-fastened connections located at the chord stud web in sheathed specimens seem to be less subjected to shear load since the dominated failure mode is local buckling, which means that the shear demand is shared between steel-to-steel and steel-to-OSB screw-fastened connections. This model shows that at peak load the forces on the screw-fastened connections are at its maximum magnitude at the center of the stud, but for sheathed specimens where the local buckling is the dominant failure mode, the force at the springs are transferred from the center towards the ends (mid lengths), where local buckling occurs (see Figures 10 and 12).

6. Discussion and Future Work

The proposed modeling protocol for sheathed and unsheathed built-up CFS columns using UELs and a combination of MID-based buckling mode imperfection magnitudes is successful and useful in simulating tested behavior of 17 column specimens. Test-to-predicted ratios for all fully built-up column models (A4, A8, B4, and B8) are less than 1.09, with a mean of 1.07 and a coefficient of variation of 0.02. The tested collapse modes and plastic mechanisms were adequately recreated in ABAQUS models. The use of contact in the models proves useful in maintaining post-buckling strength, as individual studs are not able to interpenetrate each other and flanges are adequately restrained by the OSB in the sheathed models in addition to the restraint provided by the fasteners. In addition, local buckling and localized failures in the web were shown to be dominant over flexural or distortional modes in all sheathed specimens, whether of single stud or built-up section type. In practice, local modes of failure are desirable as significant post-buckling reserve is present and excessive deformations of sheathing and walls in general are not expected to occur. The models could allow these localized failure modes to develop and could also show stress

distributions in the sheathing as the stud flanges interact with the OSB through contact and through the UELs, even though these stress fields may not be clear in Figures 10 and 12.

With validated FE models, further analyses can be completed. Namely, the nonlinear cyclic response of chord studs in shear walls could be characterized to more accurately model the CFS shear wall behavior so that the role of gravity load in the performance of these structural elements would be explored and their sensitivity to fastener-based and member-based limit states would be studied. In addition, as many lipped channel section webs are perforated in CFS structures, the effect of perforations on built-up column strength should also be investigated using this modeling framework. Also, with a minor change in boundary condition and loading scheme, built-up beam sections can be studied as well with the intent of improving AISI S100 design guidelines for all built-up members. Lastly, modeling using FE meshes developed using true stud geometry (directly from laser scan point clouds) rather than a combination of elastic buckling mode shapes as geometric imperfections is now underway by the second author, and results will be compared with MID-based imperfection combinations in a separate study.

The capacity of built-up components from a constructability point of view should also be studied further. Liao et al. (2017) investigated the distortional and local buckling and collapse behavior of unsheathed built-up CFS stub columns of varying cross-section arrangements and found that the capacities of built-up sections in compression were always less than the sum of the axial capacities of all individual studs in the built-up section. Apart from confirming that local buckling is unavoidable in built-up sections with any fastener layout, Liao et al. (2017) and Li et al. (2014), as well as the authors of this paper, saw experimentally that proper column end conditions can prevent premature buckling of individual studs. When multiple studs in one section are installed within tracks and then loaded, and subsequently if one stud is slightly longer than the other or has an initial imperfection different from the others, then that stud will initially be stressed a greater amount and will buckle first. A reduction in the entire built-up section capacity is then inevitable. Therefore, in future work, load sharing of studs that may have slightly different buckling capacities must be studied using better fastener layouts and enhanced end conditions so that a robust design paradigm for built-up CFS sections can be developed.

7. Conclusions

The intent of the work presented herein is to introduce new and advanced methods of FE modeling for CFS members, specifically applied to built-up CFS columns. Particularly, user-defined elements (UELs) are useful for modeling screw fasteners cyclic behavior using empirical fastener data and a Pinching4 framework. Output of force and displacement for each fastener is possible and can be useful when considering optimal fastener arrangements; this method of modeling fasteners can be more useful than using simple constraints or linear springs, as is typical in most previous modeling work. A simple approach to modeling stud-to-track connections is also shown to compare well with tested behavior, and overall, the modeling protocol is shown to accurately simulate tested conditions and behavior. Ongoing work will aim to understand cyclic behavior of built-up CFS chord studs, consider perforations in the lipped channel sections, use new modeling approaches for geometric imperfections, and propose improvements for fastener layouts and overall chord stud design.

Acknowledgements

Research for this paper was conducted with partial U.S. Government support under FA9550-11-C-0028 and awarded by the Department of Defense, Air Force Office of Scientific Research, National Defense Science and Engineering Graduate (NDSEG) Fellowship, 32 CFR 168a. Any opinions, findings, and conclusions or recommendations expressed in this material are those of the author(s) and do not necessarily reflect the views of the sponsors or other participants.

References

- ABAQUS 6.14-2, 2014, Dassault Systèmes Simulia Corp., Providence, RI.
- AISC 360 (2010). *Specification for Structural Steel Buildings*, American Institute of Steel Construction, Chicago, IL.
- AISI S100 (2016). *North American Specification for the Design of Cold-Formed Steel Structural Members*, American Iron and Steel Institute, Washington, D.C.
- AISI S211 (2012). *North American Specification for Cold-Formed Steel Framing - Wall Stud Design*, American Iron and Steel Institute, Washington, D.C.
- American Society for Testing and Materials (ASTM), Standard Test Methods and Definitions for Mechanical Testing of Steel Products (ASTM370-12a), ASTM, West Conshohocken, PA, 2012.
- Berwick, B. and Williamson, E. (2014). "Computational Modeling of Steel Stud Wall Systems for Applications to Blast-Resistant Design." *Journal of Structural Engineering*, 140 (8), A4014007.
- Craveiro, H.D., Paulo, J., Rodrigues, C., and Laím, L. (2016). "Buckling resistance of axially loaded cold-formed steel columns." *Thin-Walled Structures*, 106, 358-375.
- Ding, C. *Monotonic and Cyclic Simulation of Screw-Fastened Connections for Cold-Formed Steel Framing*. M.S. Thesis, Virginia Polytechnic and State University; 2015.
- Fratamico, D.C., Torabian, S., Schafer, B.W. (2015). "Composite Action in Global Buckling of Built-Up Columns Using Semi-Analytical Fastener Elements." Proceedings of the Annual Stability Conference, Structural Stability Research Council, Nashville, TN.
- Fratamico, D.C., Torabian, S., Rasmussen, K.J.R., Schafer, B.W. (2016). "Experimental Studies on the Composite Action in Wood-Sheathed and Screw-Fastened Built-Up Cold-Formed Steel Columns." Proc. of the Annual Stability Conference, Structural Stability Research Council, Orlando, FL.
- Georgieva, I., Schueremans, L., Pyl, L. (2012). "Composed columns from cold-formed steel Z-profiles: Experiments and code-based predictions of the overall compression capacity." *Engineering Structures*, 37, 125-134.
- Georgieva, I., Schueremans, L., Pyl, L., Vandewalle, L. (2012). "Experimental investigation of built-up double-Z members in bending and compression." *Thin-Walled Structures*, 53, 48-57.
- Georgieva, I., Schueremans, L., Pyl, L., Vandewalle, L. (2012). "Numerical study of built-up double-Z members in bending and compression." *Thin-Walled Structures*, 60, 85-97.
- Georgieva, I., Schueremans, L., Vandewalle, L., Pyl, L. (2012). "Design of built-up cold-formed steel columns according to the direct strength method." *Procedia Engineering*, 40, 119-124.
- Kechidi, S. and Bourahla, N. (2016). "Deteriorating hysteresis model for cold-formed steel shear wall panel based on its physical and mechanical characteristics." *Thin-Walled Structures*, 98(Part B), 421-430.
- Liao, F., Wu, H., Wang, R., Zhou, T. (2017). "Compression test and analysis of multi-limbs built-up cold-formed steel stub columns." *Journal of Constructional Steel Research*, 128, 405-415.
- Lowes, L.N., Mitra, N., and Altoontash, A. (2004). *A Beam-Column Joint Model for Simulating the Earthquake Response of Reinforced Concrete Frames* (Report #2003/10). Retrieved from the Pacific Earthquake Engineering Research Center (PEER), Berkeley, CA.
- Maia, W.F., Vieira, L.C.M., Schafer, B.W., and Malite, M. (2016). "Experimental and numerical investigation of cold-formed steel double angle members under compression." *Journal of Constructional Steel Research*, 121, 398-412.
- MATLAB 2016a, The MathWorks, Inc., Natick, MA, United States.
- Moen, C.D., Tao, F., and Cole, R. (2016). "Monotonic and Cyclic Backbone Response of Single Shear Cold-Formed Steel Screw-Fastened Connections." Proc. of the International Colloquium on Stability and Ductility of Steel Structures, Timisoara, Romania.
- Schafer, B.W. and Ádány, S. (2006). "Buckling analysis of cold-formed steel members using CUFSM: conventional and constrained finite strip methods." Proc. of the 18th International Specialty Conference on Cold-Formed Steel Structures, Orlando, FL.
- Schafer, B.W., Li, Z., and Moen, C.D. (2010). "Computational modeling of cold-formed steel." *Thin-Walled Structures*, 48, 752-762.

- Stone, T.A. and LaBoube, R.A. (2005). "Behavior of cold-formed steel built-up I-sections." *Thin-Walled Structures*, 43(12), 1805-1817.
- Tao, F., Cole, R., and Moen, C.D. (2016). "Monotonic and Cyclic Backbone Response of Single Shear Sheathing-to-Cold-Formed Steel Screw-Fastened Connections." Proc. of the Wei-Wen Yu International Specialty Conference on Cold-Formed Steel Structures, Baltimore, MD.
- Vieira, L.C.M. *Behavior and Design of Sheathed Cold-Formed Steel Stud Walls Under Compression*. Ph.D. Thesis, The Johns Hopkins University; 2011.
- Ye, J., Feng, R., Chen, W., and Liu, W. (2016). "Behavior of cold-formed steel wall stud with sheathing subjected to compression." *Journal of Constructional Steel Research*, 116, 79-91.
- Ye, J., Wang, X., and Zhao, M. (2016). "Experimental study on shear behavior of screw connections in CFS sheathing." *Journal of Constructional Steel Research*, 121, 1-12.
- Zeinoddini, V.M. and Schafer, B.W. (2012). "Simulation of geometric imperfections in cold-formed steel members using spectral representation approach." *Thin-Walled Structures*, 60, 105-117.
- Zhang, J. *Cold-formed steel built-up compression members with longitudinal stiffeners*. Ph.D. Thesis, The University of Hong Kong; 2014.
- Zhao, X. *Measurement and Application of Geometric Imperfections in Cold-Formed Steel Members*. Ph.D. Thesis, The Johns Hopkins University; 2016.
- Zhao, X., Tootkaboni, M., Schafer, B.W. (2015). "Development of a Laser-Based Geometric Imperfection Measurement Platform with Application to Cold-Formed Steel Construction." *Experimental Mechanics*, 55, 1779-1790.